Nonlinear Analysis of the Influence of Tire Inflation Pressure on Nose Landing Gear Shimmy

Phanikrishna Thota*, Bernd Krauskopf† , Mark Lowenberg‡

Faculty of Engineering, University of Bristol, Bristol, UK, BS8 1TR

and Etienne Coetzee

Airbus UK, Filton, Bristol, UK, BS99 7AR

Abstract

In this work we investigate shimmy oscillations in the nose landing gear of a passenger aircraft and study how they depend on changes in the tire inflation pressure. To achieve this, we consider a mathematical model of a landing gear that includes the influence of the tire pressure via different tire properties, such as cornering force and contact patch length. Experimental data obtained from two radial tires is used as a basis for modeling the influence of inflation pressure on tire properties. Bifurcation analysis of the mathematical model was then be performed. It yields stability diagrams in the plane of velocity and vertical force for different values of the tire inflation pressure. Specifically, we present two-parameter bifurcation diagrams for five different inflation pressures. This allows us to conclude that, for the type of tires considered, the landing gear is less susceptible to shimmy oscillations at higher than nominal inflation pressures.

*Department of Engineering Mathematics.
†Department of Engineering Mathematics.
‡Department of Aerospace Engineering.

Nomenclature

$c_\psi =$ torsional damping of strut

$c_\delta =$ lateral bending damping of strut

$c_c =$ generic damping coefficient of elastic tire

$c_t =$ torsional damping coefficient of elastic tire

$c_l =$ lateral damping coefficient of elastic tire

$d =$ vertical deflection of elastic tire

$\tilde{d} =$ normalized vertical deflection of elastic tire

$e =$ caster length

$e_{\text{eff}} =$ effective caster length

$F_z =$ vertical load on the gear

$F_{z_{\max}} =$ maximum vertical load on the gear

$\tilde{F}_z =$ normalized vertical load on the gear

$F_{K_\lambda} =$ lateral tire force or cornering force

$\tilde{F}_{K_\lambda} =$ normalized lateral tire force or cornering force

$h =$ contact patch length of elastic tire

$I_z =$ moment of inertia of strut w.r.t Z-axis

$I_y =$ moment of inertia of strut w.r.t Y-axis

$k_\alpha =$ self-aligning coefficient of elastic tire

$k_\lambda =$ restoring coefficient of elastic tire

$k_\psi =$ torsional stiffness of strut

$k_\delta =$ lateral bending stiffness of strut

$l_g =$ gear height

$L =$ tire relaxation length

$M_{K_\psi} =$ moment due to stiffness in the torsional mode

$M_{D_\psi} =$ moment due to damping in the torsional mode

$M_{K_\delta} =$ moment due to stiffness in the lateral bending mode

M_{D_δ} = moment due to damping in the lateral bending mode

M_{D_α} = moment due to tire lateral damping

M_{K_α} = self-aligning moment due to tire force

$\tilde{M}_{K_\alpha}$ = normalized self-aligning moment due to tire force

M_{λ_δ} = coupling moment between the tire deformation and lateral mode

p = tire inflation pressure

p_n = nominal tire inflation pressure

$\tilde{p}$ = normalized tire inflation pressure

R = radius of unloaded nose wheel tire at $\tilde{p}$

V = forward velocity of the aircraft

w = width of the unloaded tire at the nominal tire inflation pressure

α_m = self-aligning moment limit

γ = wheel tilt or camber angle

δ = lateral bending angle

ψ = torsion angle

ϕ = rake angle

θ = swivel angle

Introduction

Aircraft landing gears may experience torsional and lateral vibrations, known as *shimmy oscillations*, during their ground operations. Such oscillations typically occur due to a variety of flexibilities in both structural components and the tires.[1–4, 10] Shimmy oscillations can reduce stability of the landing gear and also cause wear that affects its long-term durability. In a few cases, especially during take-off and landing stages, such oscillations may be so severe that they hinder the pilot's ability to read the instrument panel accurately[5, 6 a].

[a] Airbus internal customer service reports.

Table 1. System parameters and their values as used in the tire modeling.

Tire property	*Definition*	*Symbol*
Contact patch length	The length of the tire measured along its circumference that is in contact with the ground.	$h(\tilde{p})$
Relaxation length	The distance the tire has to travel to realize the restoring force induced by a certain lateral and/or torsional deformation.	$L(\tilde{p})$
Cornering force	The lateral force developed at the tire-ground contact due to either steering or tilting of the wheel.	$F_{K_\lambda}(\tilde{p})$
Self-aligning moment	The restoring moment responsible for aligning the wheels with the direction of the vehicle (aircraft) motion.	$M_{K_\alpha}(\tilde{p})$
Torsional damping	The tire property that is responsible for reducing the amplitude of torsional oscillations.	$c_t(\tilde{p})$
Lateral damping	The tire property that is responsible for reducing the amplitude of lateral oscillations.	$c_l(\tilde{p})$

It has long been established that properties of the tire are important for the ground performance of an aircraft. Table 1 shows a list of tire properties that play a role in airliner performance. In turn, these properties are influenced by the tire inflation pressure, which is a tire parameter that can be changed easily during the operation of an aircraft. Changes in tire inflation pressure have different effects on different tire characteristics, influencing the performance of the aircraft in ways that are not well understood. Moreover, in regular aircraft operations, tire inflation pressure is a parameter that is typically checked and changed to the appropriate nominal value if the landing gear experiences shimmy oscillations. This forms the motivation for this work where the influence of tire inflation pressure on the stability of a landing gear is studied.

Specifically, the question of how the tire inflation pressure influences the occurrence of aircraft nose landing gear shimmy is considered. To this end, we start from the mathematical model presented in Ref. [8], which considers the interaction of two vibrational modes, the torsional and the lateral bending modes. In particular, geometric (coupling) effects of a non-zero rake angle ϕ of the strut with the ground are incorporated. The kinematics of the tire is modeled with a variant of the stretched string model by von Schillipe and Dietrich,[13] which accommodates the influence of the lateral bending mode on the kinematics of the tire.

In the past, a few works investigated the influence of inflation pressure on the ground dynamics of an aircraft but not in the context of shimmy analysis. An example of such past research is the aircraft ground handling study by Klyde, Magdaleno and Reinsberg,[7] who analyzed experimental data from a navy jet trainer in both time and frequency domains and concluded that tires with higher than nominal inflation pressure showed better ground handling qualities. Another important and comprehensive study on the mechanical

properties of pneumatic tires used in aircraft is the work by Smiley and Horne.[11] The authors perform a study of the tire properties for several different types of tire and also for a variety of vertical loads. Some of the tire properties are also investigated as functions of tire inflation pressure. Smiley and Horne also give empirical relationships for several different properties that are derived from the experimental data for both static and rolling tires.

The effect of tire inflation pressure on tire properties has also been studied in the case of smaller tires (for example, car or motorbike tires) than the ones used in typical airliners. Kasprzak, Lewis and Milliken[15,16] studied the effects of inflation pressure on tire properties to improve the accuracy and adaptability of the *Radt/Milliken* nondimensional tire model.[17] Similar experimental studies have been performed by Ramji, Goel and Saran[18] on small-sized pneumatic tires. Specifically, they investigated the influence of tire parameters such as tire size, ply rating, vertical load and tire inflation pressure on vertical, lateral, longitudinal and torsional stiffnesses. It is important to note that the experiments performed in both these studies involved vertical loads that are orders of magnitude smaller than those of a typical mid-size passenger airliner. Overall, no comprehensive theory exists to model the influence of tire inflation pressure for all tires, especially the ones used in modern aircraft.

The key for the work presented here is to determine and model the dependence of the tire parameters shown in Table 1 on inflation pressure. Note that this is a difficult modeling problem; for example, different makes of tire (radial ply vs bias ply) react differently to a change in tire inflation pressure. This means that equations that model the relationship between tire inflation pressure and tire parameters obtained for one tire may not necessarily be representative of a different make of tire. Therefore, our starting point is experimental data from two radial tires as used on an aircraft nose wheel. Specifically, from the experimental data we derive (normalized) mathematical equations that model the properties of the tire as functions of the tire inflation pressure. With these functions, the tire inflation pressure itself becomes an operational parameter in the mathematical model, so that we are able to study its influence on the occurrence of shimmy oscillations. In particular, we are interested in the effect of tire inflation pressure on the interaction between the torsional and lateral vibration modes that may result in different types of shimmy oscillations.

To investigate the question of how tire pressure influences shimmy oscillations, we perform bifurcation analysis with the software package AUTO.[14] Specifically, we compute two-parameter bifurcation diagrams in the velocity versus vertical force plane that depict the onset of different types of shimmy oscillations for five different inflation pressures. Such bifurcation diagrams give a comprehensive insight into the effect of tire inflation pressure on different types of shimmy oscillations.

This manuscript is organized as follows. Section I discusses the mathematical model of a nose landing gear, with special emphasis on the effect of tire inflation pressure on the tire properties. Section II presents

the nonlinear analysis of the mathematical model for varying inflation pressures. Finally, Sec. III summarizes the results and points to future work in the field of shimmy oscillations.

I. Mathematical model

The mathematical model of the nose landing gear considered here is that presented in Thota *et al.*[8] The new element is the inclusion of the tire inflation pressure as an independent parameter. Specifically, in the current work, we model the tire properties given in Table 1 as functions of the tire inflation pressure.

The model has two geometrical degrees of freedom: first, the gear may rotate about the strut axis giving rise to the *torsional mode* described by the torsion angle ψ (rad), and second, the gear may bend about an axis parallel to the fuselage centerline giving rise to the *lateral mode* which, to first-order approximation, is given by the angle δ (rad). A mathematical description of the torsional and lateral bending modes and the coupling between them is given by the equations

$$I_\psi\ \ddot{\psi} + M_{K_\psi} + M_{D_\psi} + M_{K_\alpha}\left(\tilde{p}\right) + e_{\text{eff}}\ F_{K_\lambda}\left(\tilde{p}\right) + M_{D_{\alpha\psi}}\left(\tilde{p}\right) - F_z\ \sin\left(\phi\right)\ e_{\text{eff}}\ \sin(\theta) \;=\; 0, \tag{1}$$

$$I_\delta\ \ddot{\delta} + M_{K_\delta} + M_{D_\delta} + M_{\lambda_\delta}\left(\tilde{p}\right) + M_{D_{\alpha\delta}}\left(\tilde{p}\right) - F_z\ e_{\text{eff}}\ \sin(\theta) \;=\; 0, \tag{2}$$

$$\dot{\lambda} + \frac{V}{L\left(\tilde{p}\right)}\lambda - V\ \sin\left(\theta\right) - l_g\ \dot{\delta}\ \cos(\delta) - \left(e_{\text{eff}} - h\left(\tilde{p}\right)\right)\ \cos\left(\theta\right)\ \dot{\psi}\ \cos\left(\phi\right) \;=\; 0. \tag{3}$$

Equation (1) and Eq. (2) model the torsional and lateral vibrational modes of the gear, which have moments of inertia I_ψ and I_δ, respectively. Equation (3) describes the nonlinear kinematic relationship between the torsion angle ψ, lateral bending angle δ and the lateral deformation λ of the leading edge of the contact patch of the tire. The effective caster length e_{eff} is given by

$$e_{\text{eff}} = e\cos\left(\phi\right) + R\tan\left(\phi\right) + e\sin\left(\phi\right)\tan\left(\phi\right), \tag{4}$$

where, e is the mechanical trail (caster) and R is the undeformed radius of the tire. The swivel angle $\theta = \psi\ \cos(\phi)$ of the wheel differs from the steering angle ψ due to the nonzero rake angle ϕ. The second and third terms in Eqs. (1) – (2) describe the stiffness and damping of the torsional and lateral bending modes and take the form $M_{K_{\tilde{\eta}}} = k_{\tilde{\eta}}\ \tilde{\eta}$ and $M_{D_{\tilde{\eta}}} = c_{\tilde{\eta}}\ \tilde{\eta}$, where $\tilde{\eta} \in (\psi, \delta)$; see Table 2 for the values of the stiffnesses $k_{\tilde{\eta}}$ and dampings $c_{\tilde{\eta}}$ of the modes as used in our calculations. The latter terms in the equations are the coupling moments that are generated due to the interaction of the tire with the ground. In Eqs. (1)–(3), terms that depend on the tire inflation pressure are indicated by explicit dependence on the normalized pressure $\tilde{p}$; (see Table 3). A detailed description of such quantities is given in Sec. I.A.1–I.A.5. Furthermore, V is the forward velocity of the aircraft, and F_z is the vertical load it exerts on the nose landing gear. Here,

Table 2. System parameters and their values as used in the modeling.

symbol	parameter	value	
	Structure parameters		
l_g	gear height	2.5	m
e	caster length	0.16	m
ϕ	rake angle	9.0	deg (0.1571 rad)
k_ψ	torsional stiffness of strut	3.0 x 10^5	N m rad^{-1}
k_δ	lateral bending stiffness of strut	3.24 x 10^6	N m rad^{-1}
c_ψ	torsional damping of strut	110.0	N m s rad^{-1}
c_δ	lateral bending damping of strut	1.0	N m s rad^{-1}
I_ψ	moment of inertia of strut w.r.t its own axis	100.0	kg m^2
I_δ	moment of inertia of strut w.r.t axis parallel to fuselage centerline	600.0	kg m^2
	Fixed tire parameters		
R	radius of nose wheel	0.362	m
k_λ	restoring coefficient of elastic tire	0.01	rad^{-1}
α_m	self-aligning moment limit	10.0	deg (0.1745 rad)
w	tire width	0.2	m
	Pressure dependent tire parameters		
h	contact patch length	0.1–0.3	m
L	relaxation length	0.25–0.32	m
K_α	torsional stiffness coefficient	0.5–1.4	m/rad
c_t	torsional damping coefficient	0.19–0.3	
c_l	lateral damping coefficient	0.1–0.25	
	Bifurcation parameters		
F_z	vertical force on the gear	0.0-400.0	kN
V	forward velocity	0.0-250.0	m s^{-1}
$\tilde{p}$	normalized tire inflation pressure	0.6-1.4	

the influence of vertical load F_z includes not only the static weight of the remainder (fuselage, wings, etc.) of the aircraft but also the moments exerted on the gear due to its acceleration and deceleration. This type of modeling practice is also used in the literature.[2,9] Moreover, during testing of an aircraft, F_z is measured as one of the main parameters. Therefore, in our study F_z is used as an input and natural bifurcation parameter.

I.A. Effect of inflation pressure on tire parameters

We now develop mathematical relations between different tire properties and the tire inflation pressure p. To this end, we introduce the normalized tire inflation pressure as $\tilde{p} = \frac{p}{p_n}$, where p_n is the rated or nominal tire inflation pressure of the tire under consideration; i.e., $\tilde{p} = 1.0$ corresponds to $p = p_n$. Our starting point is experimental data for two radial tires that are commonly installed on nose landing gears of larger airlines. In this section, we present graphs corresponding to one aircraft tire, which are also representative of the experimental data for the other tire. The graphs shown in Secs. I.A.1–I.A.5 involve the normalized

Table 3. Normalization of tire dependent parameters.

Symbol	*Tire property*	*Definition*	*Comments*
$\tilde{d}$	Normalized vertical deformation	d/R	d is the vertical deflection of the tire
$\tilde{p}$	Normalized pressure	p/p_n	p_n is the rated nominal tire pressure
$\tilde{F}_z$	Normalized vertical force	$F_z/F_{z_{\max}}$	$F_{z_{\max}}$ is the maximum take-off load
$\tilde{F}_{K_\lambda}$	Normalized cornering force	$F_{K_\lambda}/F_{z_{\max}}$	$F_{z_{\max}}$ is the maximum take-off load
$\tilde{M}_{K_\alpha}$	Normalized self-aligning moment	$M_{K_\alpha}/F_{z_{\max}}$	$F_{z_{\max}}$ is the maximum take-off load

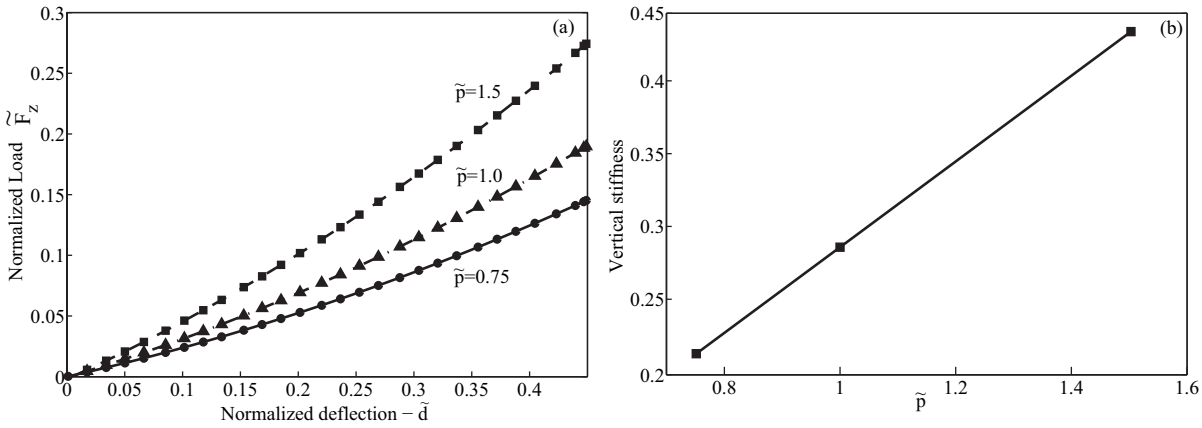

Figure 1. Panel (a) shows data of normalized vertical deflection $\tilde{d}$ of the tire as a function of the normalized vertical load $\tilde{F}_z$. The data is presented for three normalized inflation pressures as indicated. The slopes of the deflection curves at the origin give the vertical stiffness of the tire for the corresponding tire inflation pressure. Panel (b) shows the graph of the slopes of the deflection curves at the origin from panel (a) as a function of the tire inflation pressure.

quantities as defined in Table 3.

I.A.1. Contact patch length

Typically, instead of the contact patch length, vertical deflection of the tire is measured with changes in load and pressure. Figure 1(a) shows the normalized load $\tilde{F}_z$ required to produce the normalized vertical deflection $\tilde{d}$ for three different values of the normalised tire inflation pressure $\tilde{p}$. As the tire inflation pressure is increased the vertical load required to produce a given vertical deflection of the tire increases. This change is quantified in Fig. 1(b), which shows the variation of the slopes of the curves in Fig. 1(a) at $\tilde{d} = 0$ with the normalized tire inflation pressure $\tilde{p}$. The values in panel (b) correspond to the vertical stiffnesses of the tire as a function of tire inflation pressure. Figure 1(b) suggests that a linear relationship between the vertical deflection and the tire inflation pressure for a given vertical load F_z is an accurate fit for the data.

To relate vertical deflection to the length of the contact patch, we use the geometry of the deformed tire at the tire-ground contact as shown in Fig. 2. From this geometry of tire deflection, an approximate relationship between semi contact patch length h and vertical deflection d of the tire is given by

$$h(\tilde{p}) = \sqrt{R^2 - (R - d(\tilde{p}))^2}. \tag{5}$$

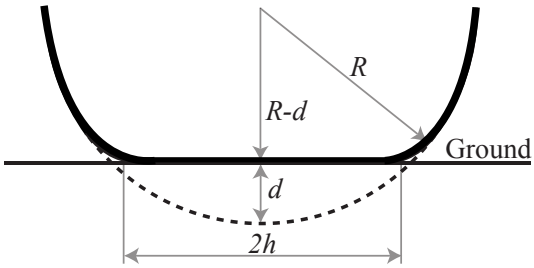

Figure 2. A schematic of tire deformation at the tire-ground contact. Here, the dashed part of the tire indicates undeformed tire in the absence of the ground.

We now use the information from Fig. 1(b) to compute the vertical deflection d for any given vertical load and inflation pressure and later substitute into Eq. (5) to compute contact patch length. Accordingly, the relationship between the semi contact patch length and tire inflation pressure for the data in Fig. 1 is given by

$$h(\tilde{p}) = R\sqrt{1 - \left(0.9 - \frac{\tilde{F}_z}{0.2943\ \tilde{p} - 0.0086}\right)^2} \tag{6}$$

I.A.2. Relaxation length

The relaxation length L for an under-inflated tire is typically higher than for an over-inflated tire,[11] that is, the relaxation length decreases with an increase in the tire inflation pressure. Even though this may hold true in the case of both radial and bias ply tires, we do not have any measured data to quantify the change in the relaxation length. Therefore, for this study we consider the relationship obtained by Smiley and Horne in Ref. [11]. It is given by

$$L(\tilde{p}) = (2.8 - 0.8\ \tilde{p})\ \left(1.0 - 2.25\ \tilde{d}\right) w, \tag{7}$$

where w is the width of the unloaded tire at the nominal tire inflation pressure $\tilde{p} = 1.0$.

I.A.3. Cornering force

Figure 3 shows the normalized cornering force $\tilde{F}_{K_\lambda}$ for three different normalized vertical loads $\tilde{F}_z$ on the gear, and for three different normalized pressures $\tilde{p}$. It is clearly seen from Fig. 3 that the maximum cornering force is significantly affected by the vertical load F_z on the landing gear. However, the value of the slip angle $\alpha \approx 12^o$ at which the maximum value occurs remains practically unchanged. This suggests that the cornering stiffness, which is the slope of the cornering force curve at $\alpha = 0$, depends heavily on the vertical load on the gear while the shape of the overall curve is maintained. On the other hand, tire inflation pressure seems to have a negligible influence on either the maximum value of the cornering force or the α value at which it occurs. (These findings are confirmed by the second tire dataset)

From the data presented in Fig. 3 we conclude that the lateral stiffness of the tire does not depend on the

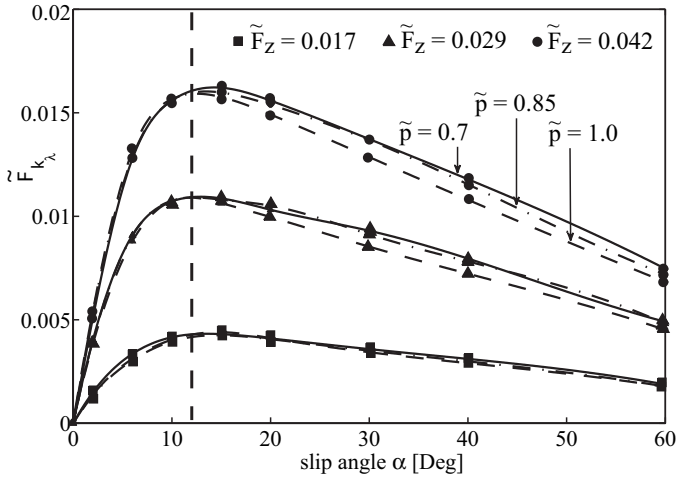

Figure 3. Normalized cornering force $\tilde{F}_{K_\lambda}$ as a function of slip angle α. Presented is experimental data for three different normalized vertical loads $\tilde{F}_z = 0.017$ (squares), $\tilde{F}_z = 0.029$ (triangles), $\tilde{F}_z = 0.042$ (circles) on the gear, and for three different normalized pressures $\tilde{p} = 0.7$ (solid), $\tilde{p} = 0.85$ (dot-dashed), and $\tilde{p} = 1.0$ (dashed).

tire inflation pressure. Here, it is important to note that we arrived at this conclusion solely by analyzing the tire data that is currently available. In the light of above discussion, for the current study we consider that the cornering force is independent of tire inflation pressure, at least for a range of pressures in the vicinity of the nominal operating pressure p_n.

Hence, as in [8], in the current study we model the cornering force F_{K_λ} by the equation

$$F_{K_\lambda}(\tilde{p}) = F_{K_\lambda} = k_\lambda \ \tan^{-1}(7.0 \ \tan(\alpha)) \ \cos\left(0.95 \ \tan^{-1}(7.0 \ \tan(\alpha))\right) \ F_z, \tag{8}$$

where the constants $k_\lambda(\tilde{p})$ represents the lateral stiffness of the tire and the slip angle α is related to the lateral deformation λ by $\alpha = \tan^{-1}(\lambda / L(\tilde{p}))$.

I.A.4. Self-aligning moment

The self-aligning moment is a direct consequence of the cornering force F_{K_λ} acting at an offset, called the pneumatic trail t_p, from the center of the tire contact patch. Now we investigate how t_p is influenced by the changes in the tire inflation pressure. Figure 4(a) shows the normalized self-aligning moment $\tilde{M}_{K_\alpha}$ for three different normalized vertical loads $\tilde{F}_z$ on the gear and for three different normalized pressures. One of the apparent features in the graph is that the slip angle α at which the self-aligning moment changes its direction from being negative to positive is practically constant for all inflation pressures and vertical loads. The self-aligning moment variations increase with an increase in the vertical load. Specifically, the maximum magnitude of the moment, which occurs at $\alpha \approx 6^o$, increases with the vertical load. The self-aligning moment is significantly influenced by changes in the pressure. Specifically, in Fig. 4(a), the maximum magnitude of the moment for a given vertical load has largest magnitude for $\tilde{p} = 0.7$ and least for $\tilde{p} = 1.0$. Therefore, the

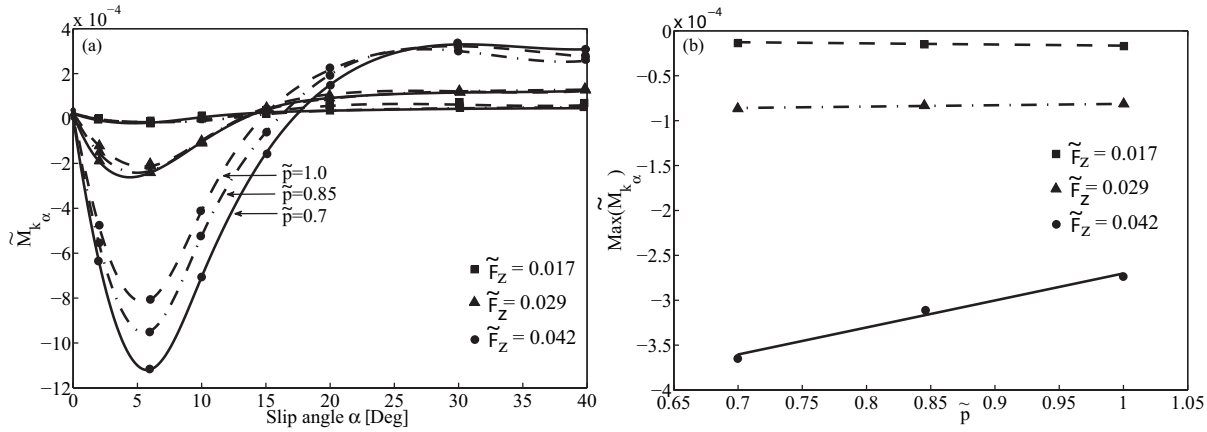

Figure 4. Normalized self-aligning moment $\tilde{M}_{K_\alpha}$ as a function of slip angle α. Here, we present experimental data for three different vertical loads $\tilde{F}_z = 0.017$ (squares), $\tilde{F}_z = 0.029$ (triangles), $\tilde{F}_z = 0.042$ (circles) on the gear and for three different normalized pressures $\tilde{p} = 0.7$ (solid), $\tilde{p} = 0.85$ (dot-dashed), and $\tilde{p} = 1.0$ (dashed).

figure suggests that as inflation pressure increases the self-aligning moment decreases. This behavior can be explained as follows: the pneumatic trail t_p, which is the moment arm to generate the self-aligning moment, decreases with increase in the tire inflation pressure. Since the cornering force is assumed to be independent of the tire inflation pressure, a reduction in the pneumatic trail t_p implies a reduction in the self-aligning moment.

For small slip angles, the cornering force acts behind the center of the contact patch, so that the self-aligning moment is stabilizing. Beyond a certain slip angle (of approx. $10^o - 15^o$, see Fig. 4(a)) the self-aligning moment changes direction and becomes a destabilizing moment. This is a direct consequence of the shifting of the point of action of the cornering force from behind the center of the contact patch to the front.

In order to quantify the effect of changing tire inflation pressure on self-aligning moment, we consider its maximum value as a function of tire inflation pressure. Here, it is sufficient to quantify just the maximum value or the slope at $\alpha = 0$. Figure 4(b) shows the maximum normalized self-aligning moment as a function of the normalized tire inflation pressure. The graph shows that the increase in the maximum normalized self-aligning moment with the tire inflation pressure is linear in nature. Note that the data for the second tire also shows the same trend.

Using the data plotted in Fig. 4(b) we are able to determine the standard model of $M_{K_\alpha}(\tilde{p})$ from[8,12] as

$$M_{K_\alpha}(\tilde{p}) = \begin{cases} (1.0823\tilde{p} - 2.0539)\,\frac{\alpha_m}{\pi}\sin\left(\alpha\frac{\pi}{\alpha_m}\right)\; F_z & \text{if } |\alpha| \le \alpha_m, \\ 0 & \text{if } |\alpha| > \alpha_m. \end{cases} \tag{9}$$

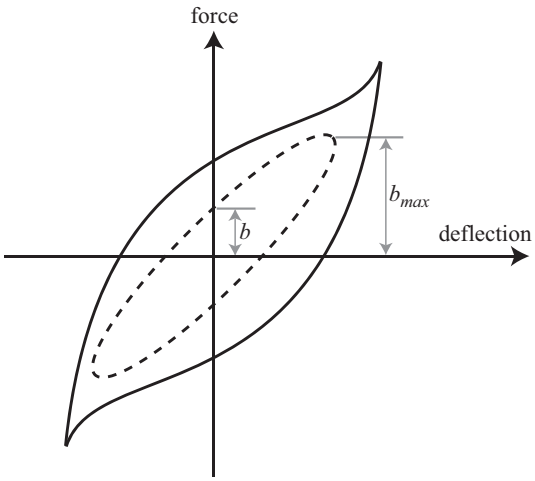

Figure 5. Schematic of a force-deflection curve where the hysteresis is due to damping.

I.A.5. Torsional and lateral damping

Damping, in general, is a difficult quantity to measure in any given system. Especially in the case of an aircraft tire, whose natural frequency of oscillation changes with the tire inflation pressure, determining the damping coefficient is quite challenging. Typically, damping characteristics are measured using a force-deflection curve, which forms a hysteresis loop due to damping, as shown in Fig. 5. The graph shows a dashed curve that represents a force-deflection curve in the case of a viscous damper. For an ideally elliptical force-deflection curve, the damping coefficient is given by

$$c_c = \frac{b}{b_{max}}. \tag{10}$$

However, in the case of aircraft tires, due to the complex nature of the inflated tires the force-deflection curves deviate from the elliptical nature of the dashed curve to take the form of the solid curve in Fig. 5. In such cases using Eq. (10) may yield a reasonable estimate of the damping coefficient, but is not necessarily very accurate. Despite its accuracy limitations Eq. (10) is commonly used to compute damping coefficients in the case of aircraft tires.

The two available sets of tire data exhibit similar force-deflection hysteresis loops and again, one is used to define the model. The experimental data in Fig. 6 representing torsional and lateral damping coefficients was obtained with Eq. (10) from hysteresis loops measured for two different tire pressures and several different vertical loads on the wheel. Figure 6(a) shows the lateral damping coefficient c_l as a function of the normalized pressure $\tilde{p}$ for different vertical loads. Since the experimental data is only available for two values of tire inflation pressure, we model the dependence of c_l on tire inflation pressure by a linear relationship; given in Eq. (12), this modeling is supported by experimental observations by Smiley and Horne.[11] Figure 6(b) shows the lateral damping coefficient c_l as a function of the normalized vertical load $\tilde{F}_z$ for two different

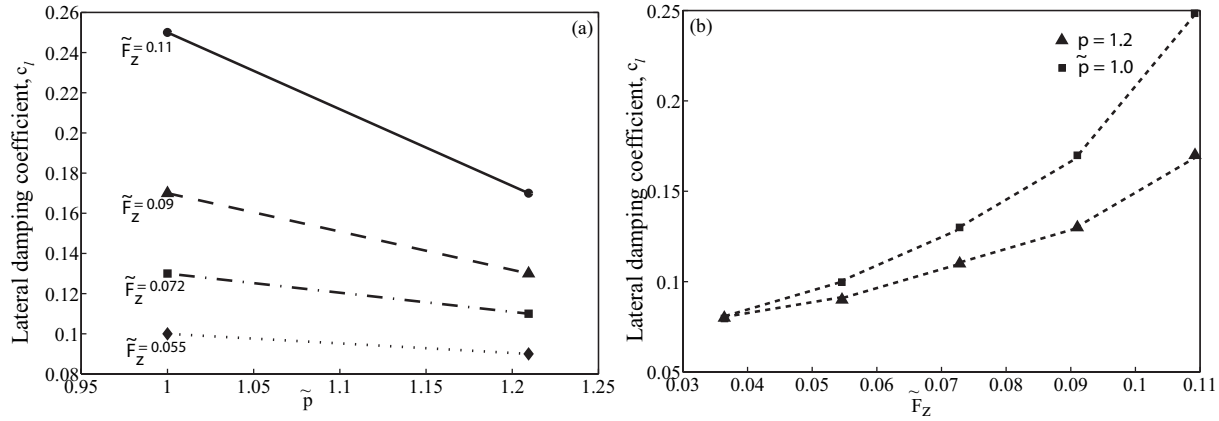

Figure 6. Panel (a) shows lateral damping coefficient c_l as a function of the inflation pressure $\tilde{p}$ for four different normalized load values $\tilde{F_z}$. Panel (b) shows the same lateral damping coefficient c_l as a function of normalized vertical load $\tilde{F_z}$. The data is presented for two different inflation pressures $\tilde{p} = 1.2$ (triangles) and $\tilde{p} = 1.0$ (squares).

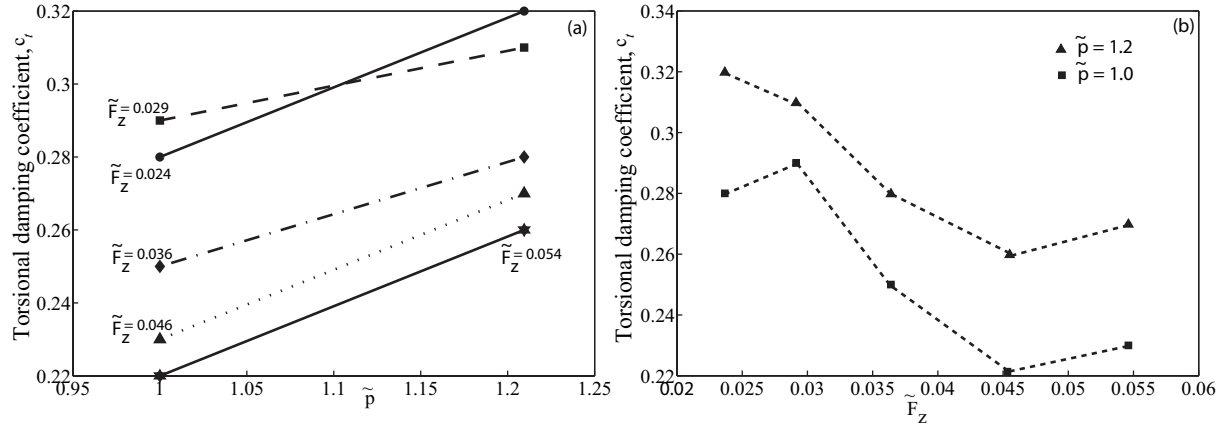

Figure 7. Panel (a) shows torsional damping coefficient c_t as a function of normalized tire inflation pressure $\tilde{p}$ for five different normalized load $\tilde{F_z}$ values. Panel (b) shows the same torsional damping coefficient c_t as a function of the vertical load $\tilde{F_z}$. The data is presented for two different inflation pressures $\tilde{p} = 1.2$ (triangles) and $\tilde{p} = 1.0$ (squares).

normalized pressures $\tilde{p} = 1.2$ and $\tilde{p} = 1.0$. The graph suggests that, for a given vertical load, the lateral damping coefficient c_l corresponding to the nominal pressure $\tilde{p} = 1.0$ is larger than for $\tilde{p} = 1.2$.

Similarly, Fig. 7(a) shows the torsional damping coefficient c_t as a function of the normalized pressure $\tilde{p}$ for different vertical loads. Again, we approximate the dependence of c_t on tire inflation pressure with a linear relationship. On the other hand Fig. 7(b) shows the torsional damping coefficient c_t as a function of the normalized vertical load $\tilde{F_z}$ for two different normalized pressures $\tilde{p} = 1.2$ and $\tilde{p} = 1.0$. Unlike in the case of lateral damping, the graph suggests that, for a given vertical load, the torsional damping coefficient c_t corresponding to the nominal pressure $\tilde{p} = 1.0$ is smaller than for $\tilde{p} = 1.2$. This behavior is very much dependent on the thickness of the tire and also the tire ply type. Overall, a combined effect of the air (or nitrogen) inside the tire along with the elastic properties of the tire create a damping effect.

Using the data from Fig. 6 and Fig. 7 we model the moment $M_{D_{\alpha\delta}}(\tilde{p})$ in Eq. (2) due to the lateral

damping of the tire given by

$$M_{D_{\alpha\delta}}(\tilde{p}) = c_l(\tilde{p})\,\frac{k_\lambda(\tilde{p})\;h^2\;F_z}{V}\;\dot{\delta}, \tag{11}$$

where the lateral damping coefficient c_l is given by

$$c_l = 0.1909\;\tilde{p} + 0.3609. \tag{12}$$

Similarly, the moment $M_{D_{\alpha\psi}}(\tilde{p})$ in Eq. (1) due to the torsional damping of the tire is represented by the equation

$$M_{D_{\alpha\psi}}(\tilde{p}) = c_t(\tilde{p})\,\frac{k_\alpha(\tilde{p})\;h^2\;F_z}{V}\;\dot{\psi}, \tag{13}$$

where the torsional damping coefficient c_t is given by

$$c_t = 0.1432\;\tilde{p} + 0.1067. \tag{14}$$

II. Bifurcation analysis of shimmy oscillations

We now perform a numerical bifurcation analysis of the dynamical system given by Eqs. (1)–(3) with the software package AUTO.[14] The main objective is to investigate the influence of tire inflation pressure on shimmy oscillations, with a special focus on the interaction between the torsional and lateral bending modes of the nose landing gear. In order to achieve this, we compute bifurcation curves that indicate the onset of shimmy oscillations as a function of aircraft velocity V and vertical force F_z. Specifically, we compute two-parameter bifurcation diagrams in the (V, F_z) parameter plane for discrete and fixed values of the normalized tire inflation pressure $\tilde{p}$.

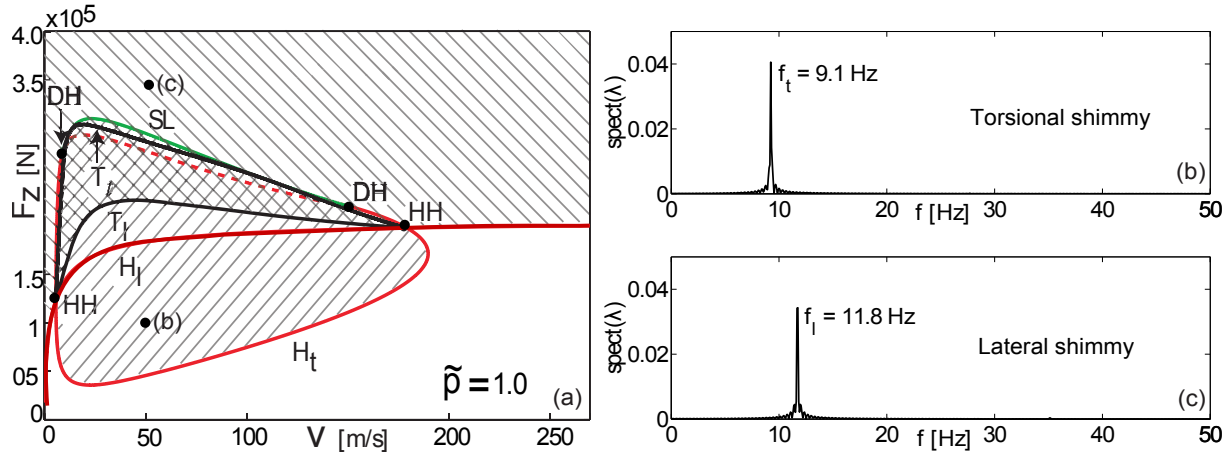

Figure 8. (a) Two parameter bifurcation diagram in the (V, F_z)-plane for Eqs. (1)–(3) for tire inflation pressure $\tilde{p} = 1.0$. In the unshaded (white) region the landing gear is shimmy-free and the straight-line rolling solution is stable. Right-slanted shading indicates torsional shimmy oscillations, and left-slanted shading indicates lateral shimmy oscillations. (b) and (c) Frequency spectra of the tire motion at the parameter values corresponding to points (b) and (c) in panel (a).

Our starting point is the bifurcation diagram for the nominal pressure case $\tilde{p} = 1.0$, which is shown in Fig. 8(a). It shows a number of bifurcation curves that divide the (V, F_z)-plane into regions corresponding to different behavior of the landing gear. The landing gear is stable and free of shimmy in the unshaded (white) part and it is unstable and experiences shimmy oscillations in the shaded region of Fig. 8(a). As we cross into the shaded region from the unshaded part via the curves H_t or H_l, either torsional or lateral bending mode undamps, giving rise to shimmy oscillations. This undamping of oscillations with a change in a parameter is called *Hopf bifurcation*. Accordingly, the Hopf bifurcation curve H_t corresponds to the onset of *torsional shimmy oscillations* that are dominated by the torsional mode; they exit in the right-slanted shading region. A frequency spectrum of the tire motion at a typical point (b) in the right-slanted shaded region of torsional shimmy is shown in Fig. 8(b). It shows a peak at the frequency $f_t = 9.1$ Hz, which corresponds to the torsional vibrational mode impling its dominance in the landing gear motion. The curve H_t forms a closed loop in the parameter space, which is often referred to as an *isola*. The isola H_t contains a solid-line segment of *supercritical Hopf* bifurcations, where the emerging shimmy oscillations are stable and a dashed-line segment of *subcritical Hopf* bifurcations that give rise to unstable shimmy oscillations. For parameter values corresponding to subcritical Hopf bifurcations the landing gear may experience a sudden jump to high-amplitude shimmy oscillations from the stable state.[8] The transition between the sub- and supercritical segments is marked by two codimension-two bifurcation points called *degenerate Hopf* points DH, where a saddle-node curve SL emerges from the Hopf curve H_t. Figure 8(a) shows that, together with the supercritical part of H_t, the saddle-node curve SL forms the boundary for torsional shimmy oscillations.

Figure 8(a) also shows a second Hopf bifurcation curve H_l. It represents the onset of *lateral shimmy oscillations*, found in the left-slanted shading region, where the lateral bending mode is dominant. Lateral shimmy oscillations occur in the region bounded below by the lateral Hopf curve H_l and also by the curve T_l (which will be discussed later), and they exist for all sufficiently large values of F_z. A frequency spectrum of the tire motion at a typical point (c) in the left-slanted shaded region of lateral shimmy oscillations is shown in Fig. 8(c); the peak at the frequency $f_l = 11.8$ Hz corresponds to the lateral mode, which implies its dominance in the landing gear motion. The two Hopf curves H_t and H_l intersect at two codimension-two double Hopf bifurcation points HH, which give rise to the torus bifurcation curves T_t and T_l. The subscript here refers to a torus bifurcation of a periodic orbit emerging from the Hopf curve H_t or H_l respectively. This suggests that *quasiperiodic shimmy oscillations* may occur for certain parameter values of V and F_z in the vicinity of the torus curves T_t and T_l. Quasiperiodic shimmy oscillations are oscillations of the landing gear in which frequency components of both the torsional and lateral bending modes are observed. In a frequency spectrum quasiperiodic shimmy oscillations are identified by two distinct peaks at both f_t and f_l as well as their differences and sums; see[8] for details. Finally, the region in the (V, F_z)-plane that contains both

left- and right-slanted shading (meshed region) indicates bistability, where both the torsional and lateral shimmy oscillations are stable. In this region, which steady state solution is observed depends on the initial condition.

Figure. 9(a)–(e) shows the change in the bifurcation curves H_t, H_l and SL as the tire inflation pressure is increased from $\tilde{p} = 0.6$ to $\tilde{p} = 1.4$ in steps of 0.2. Figure 9(c), is the case for $\tilde{p} = 1.0$ from Fig. 9. In order to facilitate comparison, we only show the curves H_t, H_l and SL in Fig. 9. Furthermore, in the panels of Fig. 9 the white region indicates a shimmy-free motion of the landing gear and the gray shaded region represents an unstable landing gear experiencing shimmy oscillations. The effect of the tire inflation pressure is apparent from extent of the gray region as the bifurcation curves in the (V, F_z)-plane change with $\tilde{p}$. Specifically, Fig. 9 shows that, as the tire inflation pressure is increased, the white region increases in size. This indicates that the landing gear is stable for a larger operating region in the (V, F_z)-plane when the tire inflation pressure is increased. In the case of the torsional Hopf curve H_t, for large tire inflation pressure, the area in the (V, F_z)-plane bounded by the isola H_t decreases. Moreover, the saddle-node curve SL, which forms the upper bound for the torsional shimmy oscillations, is always in close proximity of the isola H_t. This means that the range of velocities at which torsional shimmy oscillations occur decreases with an increase in the tire inflation pressure.

The tire inflation pressure also has a significant effect on the Hopf curve H_l corresponding to lateral shimmy oscillations. Specifically, as the tire inflation pressure is increased, the vertical load F_z at which the lateral Hopf curve H_l levels off (at ≈ 50 [m/s]) also increases. For example, while for $\tilde{p} = 0.6$ the curve H_l levels at $F_z \approx 140$ [kN], it does so only at $F_z \approx 370$ [kN] for tire inflation pressure $\tilde{p} = 1.4$. Indeed as the tire inflation pressure is increased, the curve H_l moves towards higher values of the vertical load F_z, thereby increasing the white area in the (V, F_z)-plane where the landing gear is free of lateral shimmy oscillations.

Figure 9 also shows an influence of tire inflation pressure on the region in the (V, F_z)-plane corresponding to sub- and supercritical Hopf bifurcations of torsional shimmy oscillations. As the tire inflation pressure is increased from $\tilde{p} = 0.6$ to $\tilde{p} = 1.4$, the dashed part of the isola H_t that represents subcritical torsional Hopf bifurcations decreases in length, that is, the degenerate Hopf points DH come closer to each other with an increase in $\tilde{p}$. The distance between the two points DH eventually shrinks to zero and the two points vanish for $\tilde{p} = 1.4$, making the entire isola a set of supercritical Hopf bifurcations. This suggests that for higher than nominal tire inflation pressures the landing gear is less susceptible to sudden jumps to high-amplitude shimmy oscillations in this region of parameters.

Since $\tilde{p}$ is an additional parameter, it is convenient to summarize our findings by showing a three-parameter bifurcation diagram in the $(\tilde{p}, V, F_z)$-space. It is shown in Fig. 10 and consists of surfaces H_t and H_l of Hopf bifurcations and a surface SL of saddle-node bifurcations. This three-parameter bifurcation diagram

can be builtup from the respective bifurcation curves H_t, H_l and SL for fixed values of $\tilde{p}$. Figure 10(a) shows these bifurcation curves in the $(\tilde{p}, V, F_z)$-space when the tire inflation pressure is changed from $\tilde{p} = 0.6$ to $\tilde{p} = 1.4$ in steps of 0.1. Figure 10(b) shows surfaces of bifurcations that correspond to the bifurcation curves in panel (a). In the view shown in Fig. 10(b), the region in the $(\tilde{p}, V, F_z)$-space below the surfaces H_t and H_l corresponds to a shimmy-free landing gear; the region above these surfaces, towards increasing values of the vertical force F_z, corresponds to shimmy oscillations; compare with Fig. 9. The intersection of the two Hopf surfaces H_t and H_l forms the black curves HH, which are the loci of the codimension-two double Hopf points HH; (see also Figs. 8 and 9). Furthermore, the saddle-node surface SL connects with the Hopf surface H_t along the gray curves DH.

The data and bifurcation curves presented in Fig. 9 are slices of the surfaces presented in Fig. 10(b) at the particular values of tire inflation pressure $\tilde{p}$. However, the surfaces can also be sliced, for example, for a particular velocity V to obtain bifurcation curves in the $(\tilde{p}, F_z)$-plane, or for a particular vertical force F_z to obtain bifurcation curves in the $(\tilde{p}, V)$-plane. This flexible representation of bifurcation data can be useful in the design and operational stages to evaluate and improve the performance of an aircraft landing gear.

Taken together, Fig. 9 and Fig. 10 clearly show that the landing gear is more stable for higher than nominal inflation pressures for the type of tire considered here. That is, shimmy oscillations occur on a smaller range of V and F_z values for the case of higher inflation pressures ($\tilde{p} > 1.0$) than for the case of lower than nominal inflation pressures ($\tilde{p} < 1.0$). This conclusion is in agreement with the work by Klyde, Magdaleno and Reinsberg,[7] who suggest that aircraft exhibit better ground handling properties for higher than nominal inflation pressures.

III. Summary and conclusions

We modeled and analyzed a nose landing gear typical of a commercial passenger aircraft in order to investigate the effect of tire inflation pressure on shimmy oscillations. Specifically, we developed a five-dimensional landing gear model in which the tire properties contact patch length, relaxation length, cornering force, self-aligning moment, and torsional and lateral damping coefficients change with the tire inflation pressure. In order to model the effect of inflation pressure on tire characteristics, we made use of experimental data obtained from two radial tires that are used on long haul airliner nose wheels. The data was presented in normalized quantities, which allows us to find empirical relationships between the tire inflation pressure and tire properties. We then performed a numerical bifurcation analysis of the landing gear model and compute two-parameter bifurcation diagrams in the velocity and vertical force plane for five different inflation pressures. Specifically, we computed Hopf (also torus and saddle-node in the case of $\tilde{p} = 1.0$) curves that divide the parameter space into regions of stable operation of the landing gear. This information was also

presented in the condensed form as a single three-parameter bifurcation diagram.

From our bifurcation analysis we conclude that tire inflation pressure has a significant influence on shimmy oscillations. Specifically, we find that, as the tire inflation pressure is increased, both torsional and lateral bending vibrational modes become more stable in the operational ranges of velocity and vertical force, thereby decreasing the susceptibility of the landing gear to shimmy oscillations. This behavior is apparent by the shrinking of the isola corresponding to torsional shimmy oscillations and the upward movement of the Hopf curve corresponding to the lateral shimmy oscillations. Also, as the tire inflation pressure is increased the landing gear is less susceptible to sudden jumps to high-amplitude shimmy oscillations.

One of the underlying assumptions of this work is that the normalized experimental data relating the tire inflation pressure and tire properties can be used for larger as well as smaller aircraft tires. With normalization and scaling, we applied experimental data obtained from larger aircraft tires to analyze shimmy oscillations in aircraft with smaller tires. To validate this modeling assumption, we would require a large amount of experimental and numerical data, which is very hard to obtain. However, the model that we developed in this work is quite generic in the context of investigating the effect of tire inflation pressure on shimmy oscillations. By merely altering the equations for tire properties to suit a specific tire model, one can use the landing gear model presented here to investigate shimmy oscillations in a wide variety of aircraft landing gears. Future studies will also include investigating a dual-wheel configuration in which tires on both the wheels can be inflated differently. Furthermore, the model used here can be modified to represent a main landing gear.

Acknowledgments

We thank Airbus for their financial and technical support of this research.

References

[1]Baumann, J., "A Nonlinear model for landing gear shimmy with applications to the McDonnell Douglas G/A-18A", 81^{st} *Meeting of the AGARD Structures and Materials Panel*, AGARD-R-800, 1995.

[2]Besselink, I. J. M., "Shimmy of aircraft main landing gears", *Dissertation,* University of Delft, The Netherlands, 2000.

[3]Glaser, J., and Hrycko, G., "Landing gear shimmy - De Havilland's experience", 81^{st} *Meeting of the AGARD Structures and Materials Panel*, AGARD-R-800, 1995.

[4]Krabacher, W. E., "A Review of Aircraft Landing Gear Dynamics", 81^{st} *Meeting of the AGARD Structures and Materials Panel*, AGARD-R-800, 1995.

[5]Ligum. T. I., Skripnichenko. S. Yu., and Shishmarev. A. V., "Aerodynamics of Tu-154B Aircraft [in Russian] ", *Transport*, Moscow, 1985.

[6]Plakhtienko. N. P., and Shifrin. B. M., "Critical shimmy speed of nonswiveling landing-gear wheels subject to lateral loading ", *International Applied Mechanics*, 42(9), 2006.

[7]Klyde, D. H., Magdaleno, R. E., and Reinsberg, J. G., "The Effect of Tire Pressure on Aircraft Ground Handling." *Proceedings of AIAA Atmospheric Flight Mechanics Conference,* Montery, California, USA, No. 2002-4798, 2002.

[8]Thota, P., Krauskopf, B., and Lowenberg, M., "Interaction of Torsion and Lateral Bending in Aircraft Nose Landing Gear Shimmy," *Nonlinear Dynamics*, (57)3, 2009.

[9]Tanner, J. A., Daugherty, R. H., Smith. H. C., "Mechanical properties of radial-ply aircraft tires ", *SAE transactions* 114(1), 2005.

[10]Smiley, R. F., "Correlation, Evaluation, and Extension of Linearized Theories for Tire Motion and Wheel Shimmy", NACA-1299, 1957.

[11]Smiley, R. F., and Horne, W. B., "Mechanical Properties of Pneumatic Tyres with Special Reference to Modern Aircraft Tire", NACA-4110, 1958.

[12]Somieski, G., "Shimmy Analysis of a Simple Aircraft Nose Landing Gear Model Using Different Mathematical Methods", *Aerospace Science and Technology*, 1270-9638(8), 1997.

[13]von Schlippe, B. and Dietrich, R., "Shimmying of a Pneumatic Wheel,"Naca rept. 1365, 1947.

[14]Doedel, E. J., Champneys, A. R., Fairgrieve, T., Kuznetsov, Yu., Sandstede, B., and Wang, X., "AUTO97 : Continuation and bifurcation software for ordinary differential equations,"`http://indy.cs.concordia.ca/auto/`, May 2001.

[15]Kasprzak. E. M, Lewis. K. E, and Milliken. D. L, "Inflation Pressure Effects in the Nondimensional Tire Model ", Motorsports Engineering Conference and Exhibition, Michigan, USA 2006.

[16]Kasprzak. E. M, Lewis. K. E, and Milliken. D. L, "Tire Asymmetries and Pressure Variations in the Radt/Milliken Nondimensional tire Model "Motorsports Engineering Conference and Exhibition, Michigan, USA 2006.

[17]Radt, H.S. and W.F. Milliken, Motions of Skidding Automobiles, SAE Paper Number 205A, SAE Summer Meeting, Chicago, IL, June 5-10, 1960.

[18]Ramji, K., Goel, V. K., and Saran, V. H., "Stiffness Properties of Small-sized Pneumatic Tyres ", Proc. Instn. Mech. Engrs. Vol 216 Part D: J Automobile Engineering, 2005.

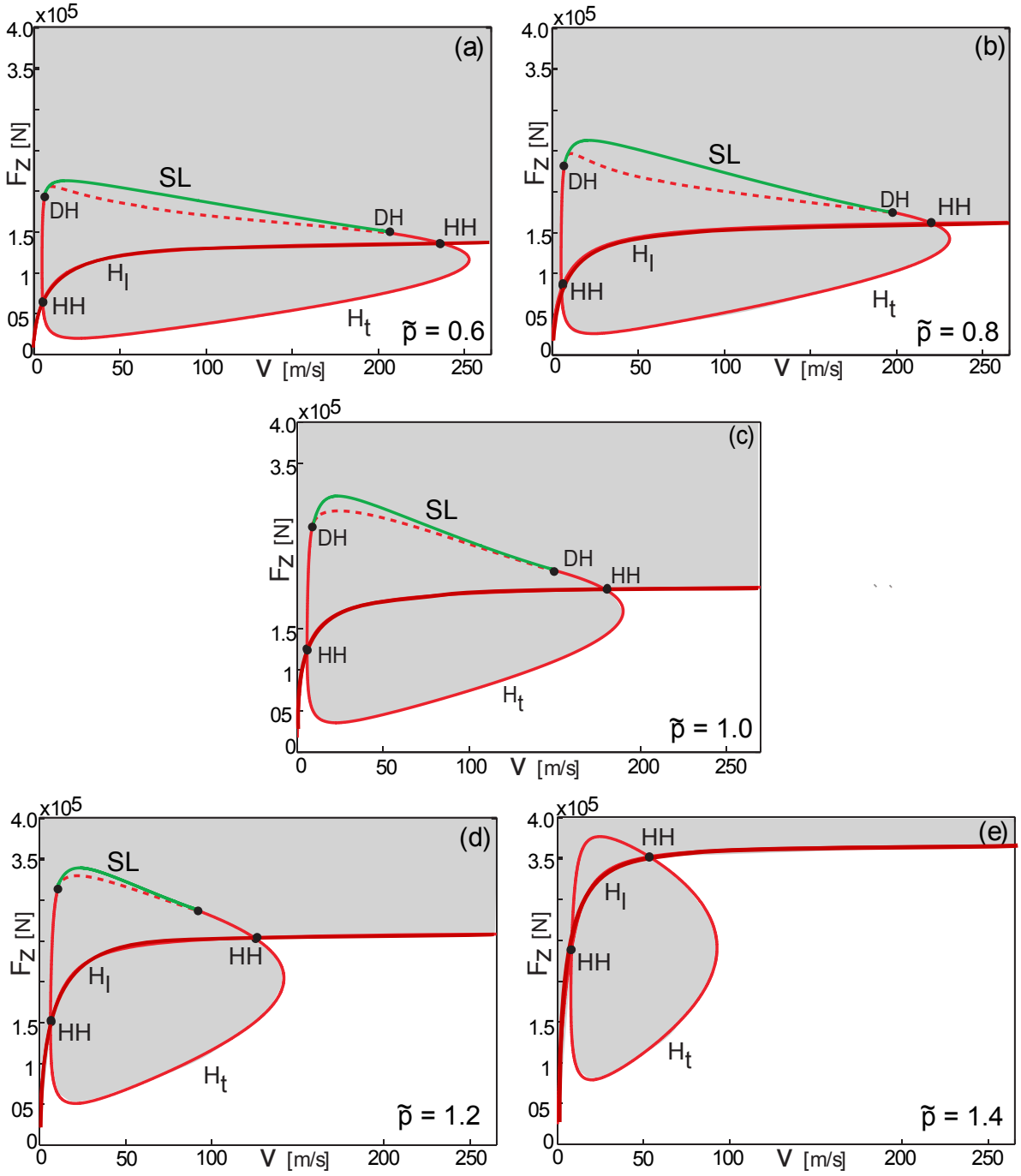

Figure 9. Two-parameter bifurcation diagrams in the (V, F_z)-plane for Eqs. (1)–(3) and for inflation pressures $\tilde{p} = 0.6$, $\tilde{p} = 0.8$, $\tilde{p} = 1.0$, $\tilde{p} = 1.2$ and $\tilde{p} = 1.4$. As indicated, all panels show the Hopf bifurcation curves H_t and H_l and the saddle-node curve SL (if it exists). Straight-line rolling is stable in the white region, and shimmy oscillations occur in the grey region.

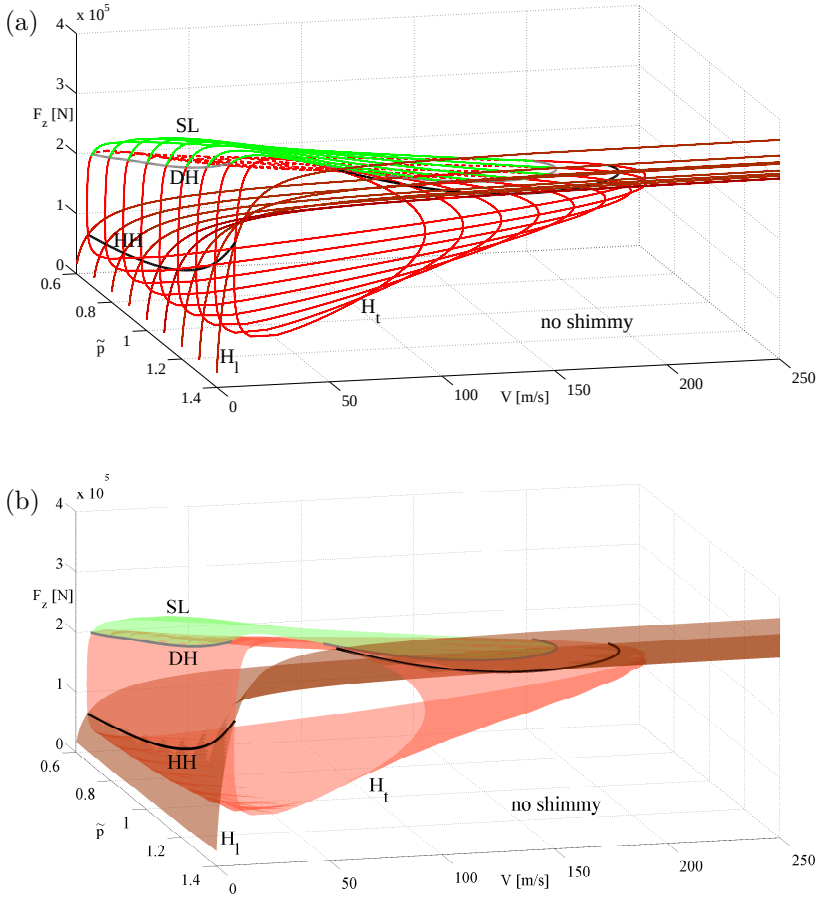

Figure 10. Three-parameter bifurcation diagram in $(\tilde{p}, V, F_z)$-space. (a) - bifurcation curves H_t, H_l and SL in $(\tilde{p}, V, F_z)$-space when the tire inflation pressure is changed from $\tilde{p} = 0.6$ to $\tilde{p} = 1.4$ in steps of 0.1. (b) - Surfaces rendered from the bifurcation curves shown in (a).